Space–time visualization of vibration of a ribbed cylinder

J Woodhouse[1]* and **J Power**[2]
[1]Department of Engineering, University of Cambridge, UK
[2]Topexpress Limited, Cherry Hinton, Cambridge, UK

Abstract: Data from an axial array of sensors along a ribbed cylindrical structure may be analysed to allow the evolving vibrational response to impulsive driving to be plotted as a function of space and time. The process is carried out separately in a series of frequency bands, by first carrying out a time–frequency analysis at each position. Aspects of the behaviour not previously discussed are highlighted by this analysis. These aspects are discussed in the light of a previously published theoretical model [**1**]. Since reflections from the cylinder's ends also play a role here, it has been necessary to develop further theoretical modelling to interpret the measurements. The new experimental approach, which is described here as the method of 'space–time cross-sections', has scope for application to other problems involving structure-borne vibration. This illustrates the power of time–frequency analysis and its extensions for engineering vibration analysis.

Keywords: time–frequency, vibration, cylinder

NOTATION

f, F	window function and its Fourier transform
n	angular order
t	time
t'	dummy time variable
v	velocity
V	sonogram signal
x, y	observation and driving points
θ	azimuthal angle
ρ	modal density
τ	half-width of the Hanning window
ϕ_k	kth mode shape
ω	frequency
ω_k	kth natural frequency

1 INTRODUCTION

A new method of processing data or displaying results can sometimes illuminate aspects of an old problem which had not previously been apparent. In earlier papers [**1**, **2**] the vibration of a cylinder stiffened by periodically placed T-section ribs was discussed, demonstrating good agreement between theory and measurements. The results are now presented of a different technique of measurement and data analysis applied to the same experimental structure, and the interpretation of these features is discussed.

The main emphasis in the previous studies was upon the pattern of stop and pass bands for wave transmission along the cylinder. These bands arise as a result of the periodically placed ribs. Their frequency ranges are different for each of the waveguide modes of propagation along the cylinder, corresponding to dependence on azimuthal angle θ of the form $\cos n\theta$, with the different values of $n = 0, 1, 2, 3, \ldots$. The pattern of stop and pass bands is summarized in Fig. 1. The structure under investigation is made of mild steel with a mean shell radius of 0.76 m, so that its ring frequency is about 1130 Hz. Thus the frequency range corresponds to about three times the ring frequency, the same range as previously discussed in detail. Pass bands, for each individual value of n, appear as vertical lines. Plotted circles correspond to band edges with a Bloch wavenumber of zero, in other words to motion such that adjacent bays deform identically. Crosses correspond to the Nyquist Bloch wavenumber, in which the deformation in adjacent bays has the same form but opposite signs. For more details of this figure, including sketches of the mode shapes of the cylinder and rib motion at various points in it, see reference [**2**].

A major element of the previous experimental investigation of this ribbed cylinder was time–frequency

The MS was received on 21 October 1999 and was accepted after revision for publication on 29 November 1999.
* *Corresponding author: Department of Engineering, University of Cambridge, Trumpington Street, Cambridge CB2 1PZ, UK*

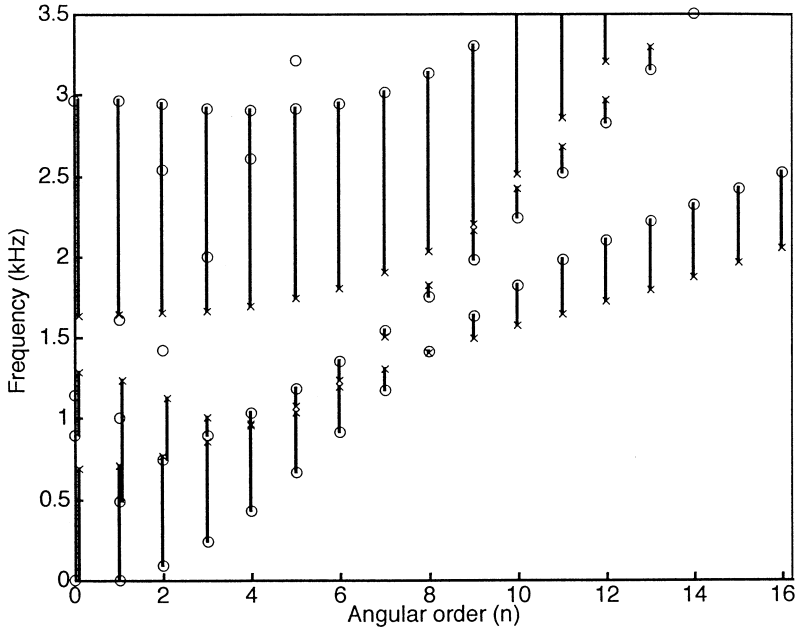

Fig. 1 Pass bands for $0 \leqslant n \leqslant 16$, for the ribbed cylinder studied here

analysis. The authors have discussed in some detail how a sonogram analysis of the impulse response of a structure measured at a point remote from the drive can give direct information about the group velocity of travelling waves, as a function of frequency [**3**]. This approach was used to give the most stringent test of the theoretical predictions for the behaviour of the ribbed cylinder, by comparing observed first-arrival times in sonograms with predicted travel times over the appropriate number of bays.

That idea will now be extended. Firstly, responses to a single impulse were measured by an array of receiving accelerometers spaced axially along the cylinder. Each of these responses was processed to give a sonogram, as discussed before. A particular frequency band can then be extracted from each sonogram in turn and assembled into a contour plot of response against time and sensor position, in other words the axial position along the cylinder. This gives a picture of the motion of any wave-packets travelling along the cylinder in the selected frequency range. Such a picture is called a 'space–time cross-section' of the family of sonograms.

Before discussing measurements on the cylinder, it is useful to consider briefly what such a picture is expected to show. This is best done by first considering a much simpler one-dimensional wave-carrying system: if an impulse is applied to a stretched string of finite length with fixed ends, the space–time response is as summarized in Fig. 2a. A pair of identical impulses travel outwards from the drive point at the wave speed for the string. As each one in turn reaches an end, it is reflected and inverted. In due course, each reaches the other end and reflects again, and so on. After one natural period of the fundamental mode of vibration of the string, the impulses pass each other at the driving point, and thereafter the pattern repeats indefinitely (in the absence of dissipation). This process is shown in the diagram, the position of the impulses on the string being plotted along the x axis and time being shown on the y axis. The two zig-zag lines represent the paths of the two impulses initiated at the point labelled A. An observer at point B, for example, would see the time history plotted in Fig. 2b, each impulse passing that point twice per cycle, with alternating signs since there is a phase inversion at each reflection from a fixed end.

For the ribbed cylinder things are less simple. There is no single wave speed at which all disturbances travel. Instead, each waveguide mode will have its own dispersive behaviour. However, in a given narrow frequency band there will in general be a well-defined group velocity for each waveguide mode able to propagate at that frequency. A pair of wave-packets travelling at that group velocity, initiated by the original impulse, should travel back and forth along the cylinder in much the same way as the travelling impulses on the string. Thus some trace of the pattern of Fig. 2a might be expected in the cross-section plots.

The details will of course be less clear than in the simple case of the string. For the experiment as described above, the different waveguide modes corresponding to different n values will all be superimposed on the diagram. This problem could be reduced by analysing data from a circumferential array of sensors to separate the different values of n, as was done in the measurements reported earlier [**2**]. However, the gain in clarity is offset by a proliferation in the number of pictures

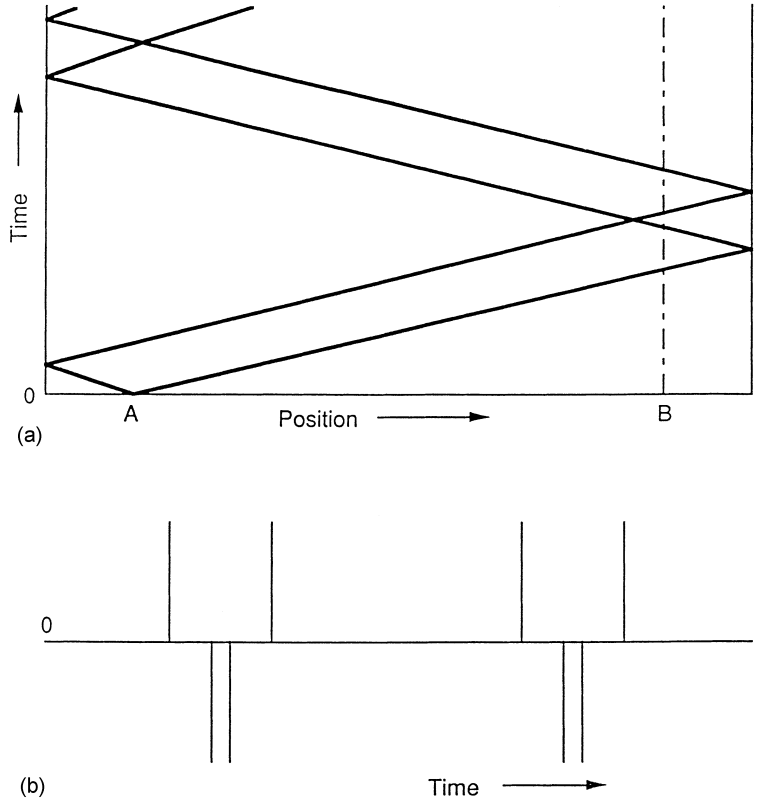

Fig. 2 (a) Space–time diagram showing the response of a stretched string to an impulse at time $t = 0$. (b) The time signal which an observer at point B would measure

needed to convey the result. It will be shown here that even without such analysis it is possible to associate observed travelling wave-packets with particular propagation mechanisms and particular angular orders. This is a consequence of the detailed theoretical study of this cylinder described in the earlier work [**1**].

2 MEASUREMENTS AND ANALYSIS

The ribbed cylinder is shown diagrammatically in Fig. 3, with an indication of the measurement positions. It has 44 nominally identical bays and a measurement was made in every bay. Measurements were in fact made reciprocally. An accelerometer was placed at the centre of bay 8 and the cylinder was then tapped in the centre of each bay using a force-transducer hammer. These tapping points were all in an axial line with the accelerometer. The force and response signals were collected by a digital data-logger, response levels were normalized according to the magnitude of each hammer blow and sonograms were calculated. A Hanning window was applied to each individual segment of data prior to Fourier analysis. It is possible that similar results could be obtained by other approaches to time–frequency analysis.

When the application of sonograms to this problem was previously described [**3**], some discussion was devoted to the trade-off between time resolution and frequency resolution. This is governed by the length of time window used for the individual fast Fourier transforms (FFTs) making up the sonogram. A longer window gives more frequency information but blurs the time variation; a shorter window has the opposite effect. The same question of how best to choose a window length arises in the context of cross-sections. Figure 4 shows three cross-sections, all at the same centre frequency but with three different lengths of time window. In each case, time is plotted on the y axis and distance along the structure on the x axis. The bottom edge of the box corresponds to the moment of application of the impulse, and the total time range is constant at 31.2 ms (as in all sonograms in the earlier paper [**2**]). The contours show intensity at 3 dB intervals. The highest contour is solid, the lower ones are broken with a progressively decreasing mark–space ratio so that there is no confusion of hills and valleys.

The driving point in bay 8 is conspicuous as the point from which signals emanate at time zero. The main feature visible in all three pictures, with more or less clarity, is the pair of slanting straight lines radiating from this point. These lines indicate travelling wave-

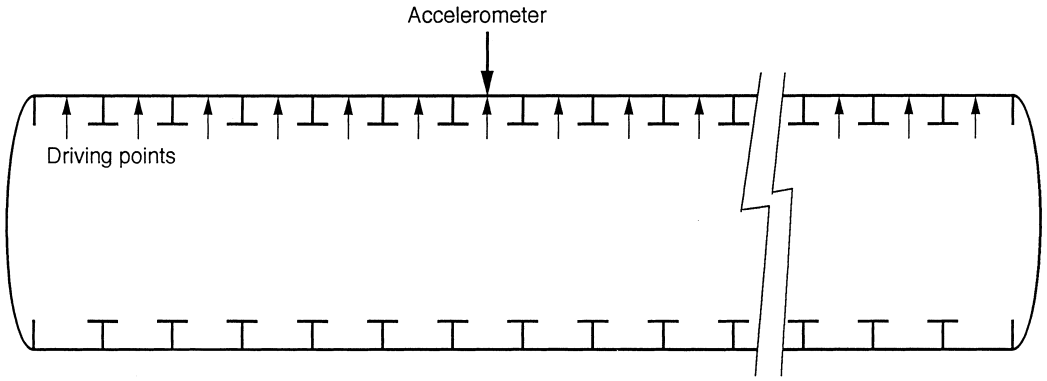

Fig. 3 Diagrammatic cross-section of the ribbed cylinder, showing the accelerometer placing in bay 8 and the excitation points at the centre of every bay

packets corresponding to the fastest group velocity within the frequency range. No clear, coherent reflections can be seen from the ends of the cylinder, even for these fastest wave-packets. The reasons for this will be discussed later. By comparing the three pictures, the influence of window length can be seen. In this case, perhaps the middle length of window gives the most useful picture. However, if a similar comparison is made at a frequency where the fastest group velocity is significantly faster or slower than it is in this case, a shorter or longer window may become preferable.

3 EXPECTED PATTERN OF GROUP VELOCITIES

Before showing a representative selection of cross-sections obtained from the measurements, a single sonogram is compared with its theoretical counterpart to see what the expected pattern of group velocities should be. Figure 5 shows a sonogram of the response in bay 20 to excitation in bay 8. Several large peaks are evident, with a broad 'horseshoe' structure in the right-hand half of the picture. This is to be compared with Fig. 6, which is a composite picture of the expected first-arrival times calculated from group velocities determined by the theoretical model described previously [**1**]. The size of each plotted symbol is a measure of the corresponding modal amplitude at the centre of a bay, where the driving and observing points were. The origin of the regions of strong signal in Fig. 5 can be seen in the theoretical picture. Generally, the areas of large amplitude in the experimental sonogram correspond to those regions of Fig. 6 with a high density of plotted points. The more prominent of these regions are marked on Fig. 6 by shading, and it is obvious that these regions have their counterparts in Fig. 5.

Figures 5 and 6 are divided into two distinct frequency regions. Below about 1.5 kHz, there are just three large peaks in Fig. 5. These correspond to the turning points in the theoretical first-arrival curves for (a) band 1, $n = 4$; (b) band 1, $n = 4$, 5 and 6; and (c) band 2, $n = 1$ and band 1, $n = 6$. The region of Fig. 5 above about 1.5 kHz shows two distinct features which are revealed by Fig. 6 to correspond to the loci of turning points for bands 1 and 3 respectively. The faster-travelling feature arises from band 3, for all values of n from zero upwards. The slower-travelling feature arises from band 1, for $n = 9$ upwards. Notice, how important the theoretical results are in giving a correct interpretation of Fig. 5. It might be tempting to suppose that the second line, following roughly parallel to the first arrival in the right half of the figure, was the result of an end reflection. Instead, it is obvious that it is the first arrival by a different propagation mechanism with a slower group velocity. This interpretation is confirmed by the cross-sections to be shown in the next section.

Figures 5 and 6 show what to expect in the cross-sections. At very low frequencies, there are only very few modes to excite and little energy is put into the structure. As frequency increases, the transmission mechanisms slow down until the break in the pictures at around 1.5 kHz. Above that frequency, the fastest mechanism, associated with band 3, rapidly increases its velocity with frequency until it reaches a value that stays roughly constant to the top of the frequency range plotted. This value corresponds approximately to the group velocity of bending waves on an infinite flat plate having the thickness of the cylindrical shell. A slower mechanism, associated with band 1 for high values of n, produces a roughly parallel series of arrivals. Towards the top end of the frequency range, most of the input energy goes into band 1 and the experimental results are dominated by this band.

4 CROSS-SECTION RESULTS

Figures 7 to 12 show a representative selection of cross-sections, in order of increasing frequency. In all cases the

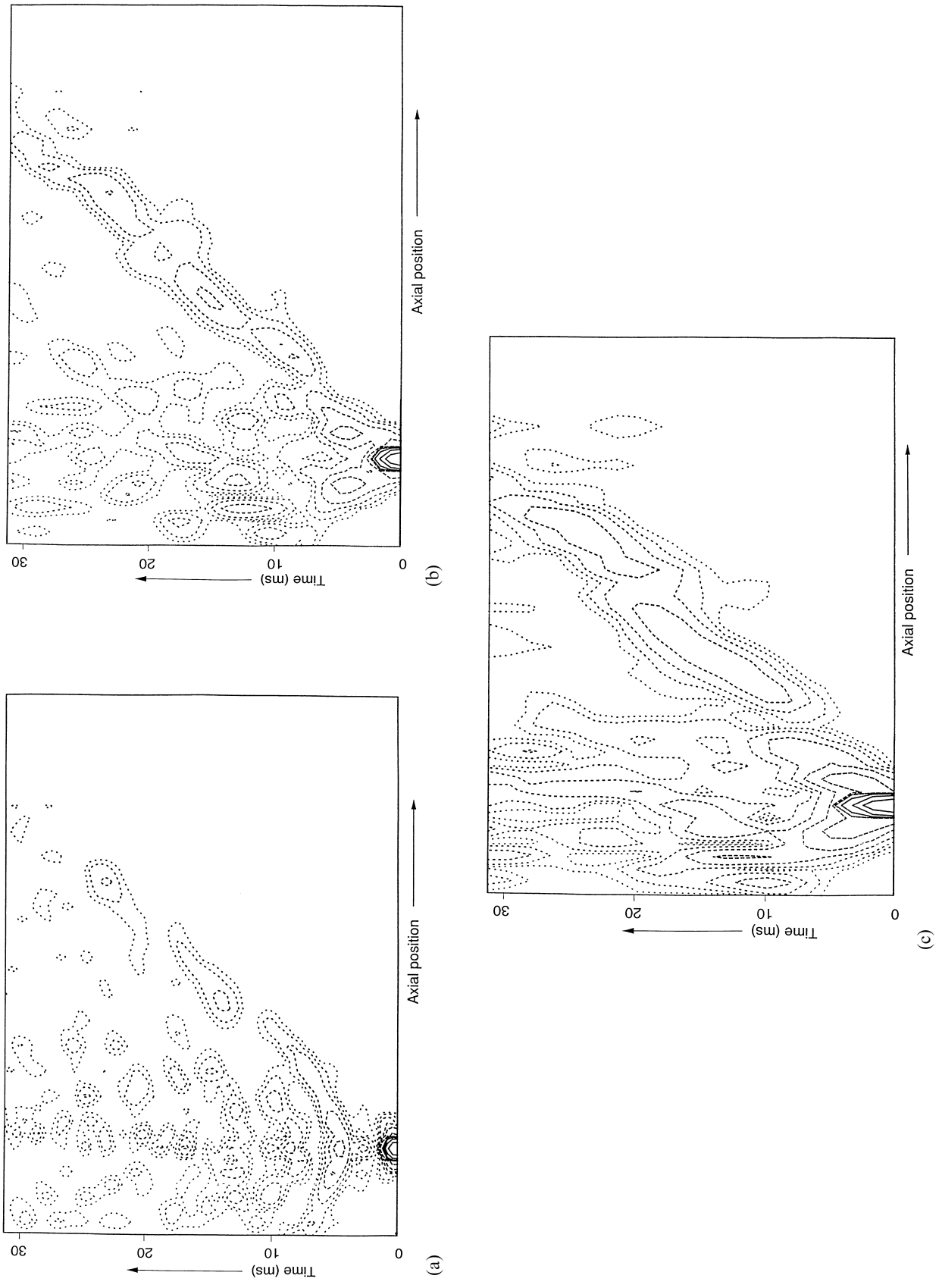

Fig. 4 The influence of the sonogram time window on cross-sections. All are centred at frequency 781 Hz, using time window lengths of (a) 3.2 ms, (b) 6.4 ms, (c) 12.8 ms

time range is the same as in Fig. 4. The contours are spaced at 3 dB intervals, auto-scaled on the highest feature in each individual picture. Lines have been drawn on the figures corresponding to visible features, which are discussed below.

Figures 7, 8 and 9 show frequencies below the break in Fig. 6. The lowest of these, Fig. 7, centred at 469 Hz, shows two pairs of radiating lines, corresponding to propagating wave-packets with two different speeds. In neither case is there much trace of coherent end reflections in the expected places, an issue which will be discussed in the next section. At a slightly higher frequency, Fig. 8 shows the expected slowing down of propagation. Here it can be seen that there is only one clear speed, and there is perhaps an indication of a reflection from the end of the cylinder closer to the driving point. By the time 1406 Hz is reached, in Fig. 9, propagation has slowed to the extent that the first arrival in bay 20 is outside the time range plotted in Figs 5 and 6. The most prominent feature of this figure is the vertical band at the position of bay 8, corresponding to a lot of vibration energy, with group velocities so slow that it stays in the immediate vicinity of the drive point for the whole time window plotted there.

For all three of these cross-sections, much of the dynamic range of the contour plot is taken up by the large peak in bay 8 near time zero. This arises from a significant 'reactive' component of the cylinder response to point driving at these low frequencies. To ensure that some other details are visible in these pictures the total number of contours has been varied, as specified in the captions. It is of some interest to examine the magnitude of this reactive response of the structure at time zero. A calculation of the expected response according to the theoretical model is given in the Appendix. This predicts an enhancement relative to the surrounding points which rises towards lower frequencies to a maximum of about 12 dB. The contour maps indeed show a rise towards lower frequencies, by an amount which seems to be a little higher than this prediction. This relatively minor discrepancy is believed to arise from some slight non-linearity somewhere in the instrumentation during the very short initial peak of acceleration at the driving point.

Figures 10, 11 and 12 correspond to frequencies above the break in Fig. 6. Figure 10, just above this break at 1562 Hz, shows traces of propagation at two different speeds together with a significant amount of response remaining close to the driving point. Figure 11, a little higher in frequency, shows clear, fast-travelling waves corresponding to the fastest propagation mechanism, associated with band 3, as discussed in the previous section. It also shows something which is met here for the first time. Clear straight lines corresponding to the feature of Fig. 5 associated with band 1 might have been expected, propagating slower than the band 3 mechanism. What is distinctive, however, is a set of horizontal lines (two of them in this figure). Careful inspection reveals that these horizontal striations end on a line which corresponds to the expected group velocity for band 1 (shown in the figure as a pair of dashed lines with shorter dashes). In other words, the striated pattern fills in a wedge whose apex lies at the driving point at time zero.

The reason for these horizontal lines lies in the fact that the frequency spacing between successive values of

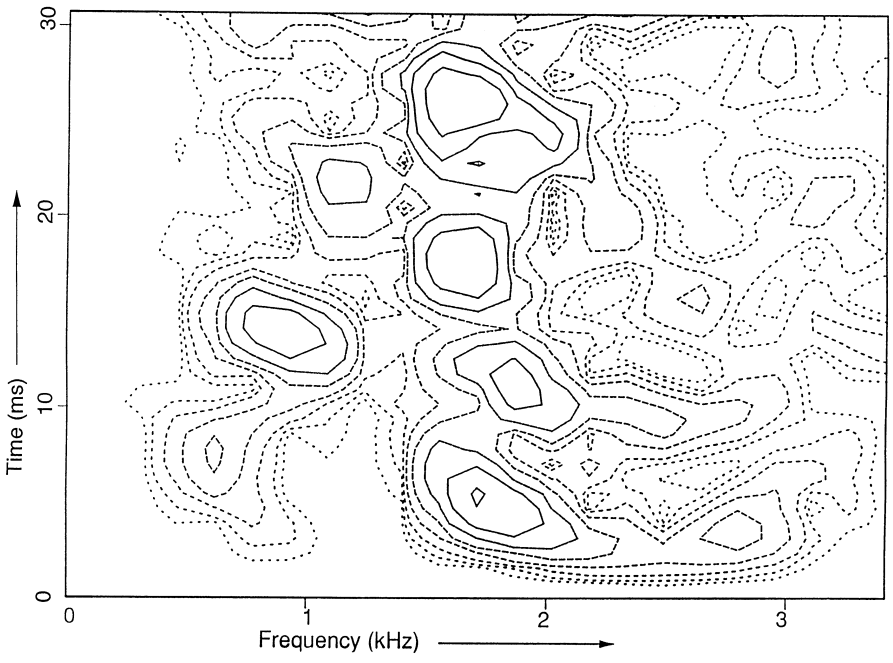

Fig. 5 Sonogram corresponding to transmission from bay 20 to bay 8

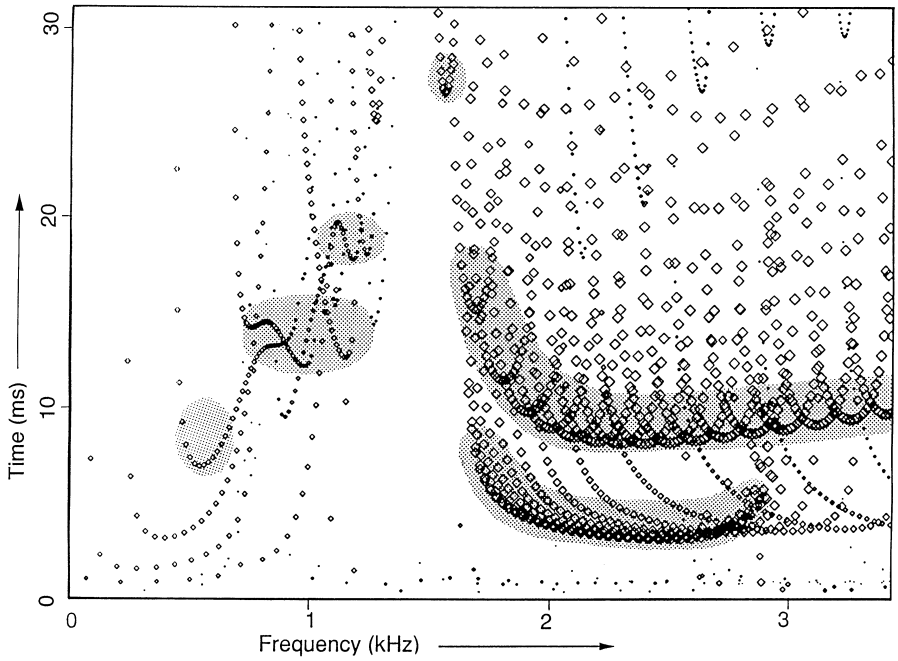

Fig. 6 Theoretical first-arrival plot for comparison with Fig. 5

n in band 1 is too small to be resolved by the frequency window in use here. Thus several values of n are seen simultaneously and beating is observed between them. Figure 6 shows that the bands for different values of n are very similar except for a frequency shift. This enables the beating effect to be very strong, since for each value of axial wavenumber, the same frequency difference will separate adjacent n modes. The reason that the response fills the whole triangle rather than being confined to the two boundary lines has to do with the narrowness of the pass bands compared with the frequency window, and will be discussed further in the next section.

The phenomenon can also be described in terms of travelling wave-packets. The circumferential component of group velocity for band 1 is determined by the

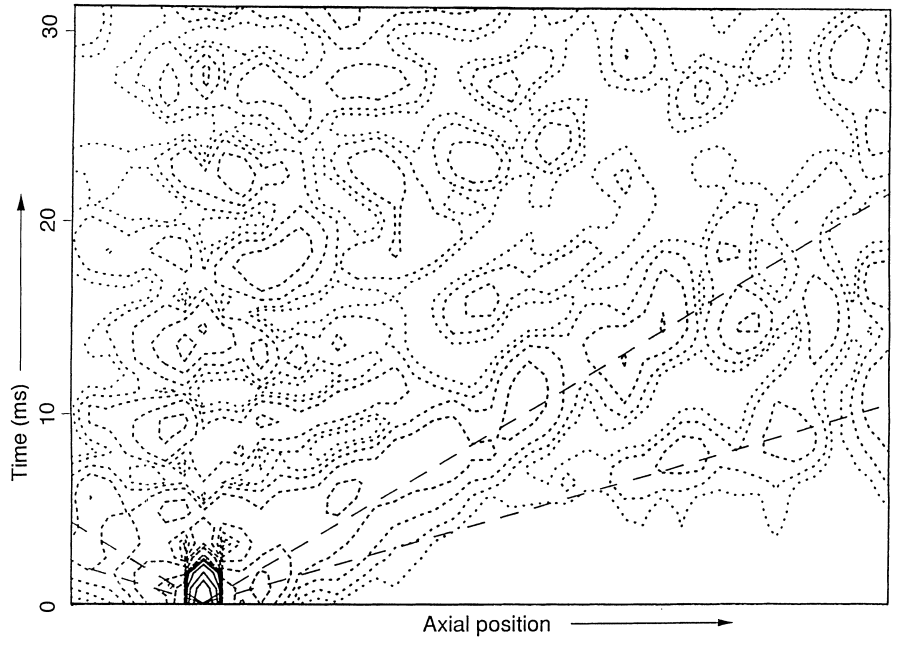

Fig. 7 Cross-section centred at 469 Hz with bandwidth 156 Hz and 12 contours spaced at 3 dB intervals

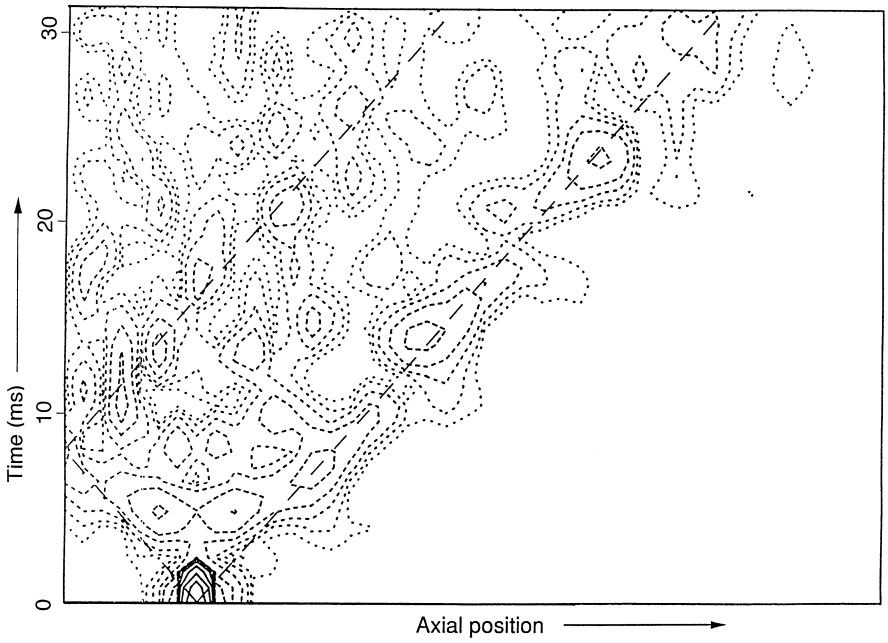

Fig. 8 Cross-section centred at 937 Hz with bandwidth 156 Hz and 10 contours spaced at 3 dB intervals

frequency spacing between the pass bands for successive n values. As just pointed out, Fig. 6 shows this spacing to be approximately constant—the successive 'horseshoes' are spaced evenly along the frequency axis. The axial component of group velocity, however, can vary from practically zero at the edges of the pass bands to values at the band centres determined by the turning points of the horseshoes. Thus the initial impulse launches waves that travel helically around the cylinder at a range of angles, from purely circumferential up to a limiting angle associated with the values of n appropriate to the given frequency range. These waves return to the line of sensors once per revolution of the cylinder, giving the set of horizontal lines.

The final cross-section (Fig. 12) shows another new effect. By this frequency, slightly above the frequency range plotted in Fig. 1, the lines associated with band 3 have disappeared from view, as discussed earlier. There

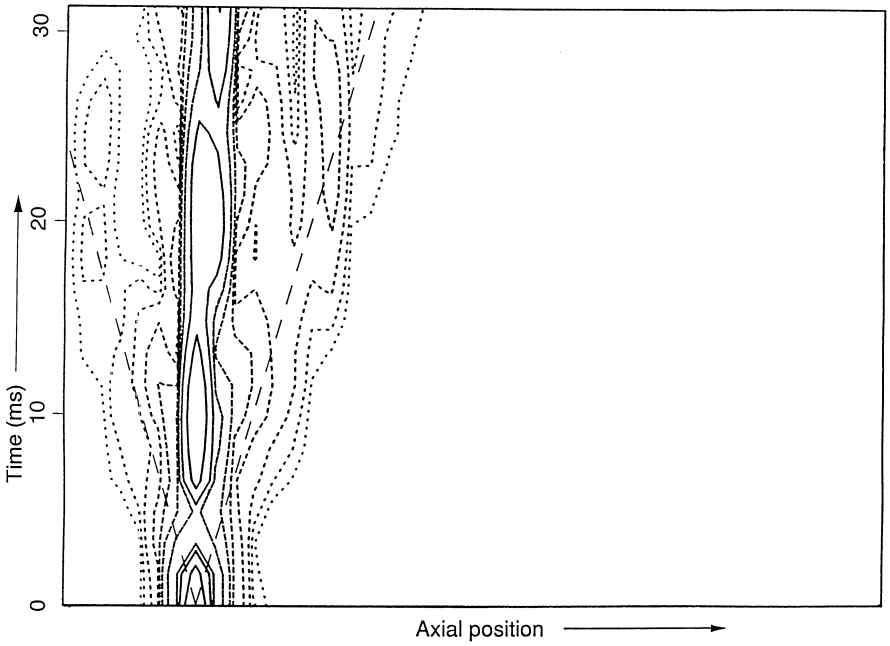

Fig. 9 Cross-section centred at 1406 Hz with bandwidth 78 Hz and 10 contours spaced at 3 dB intervals

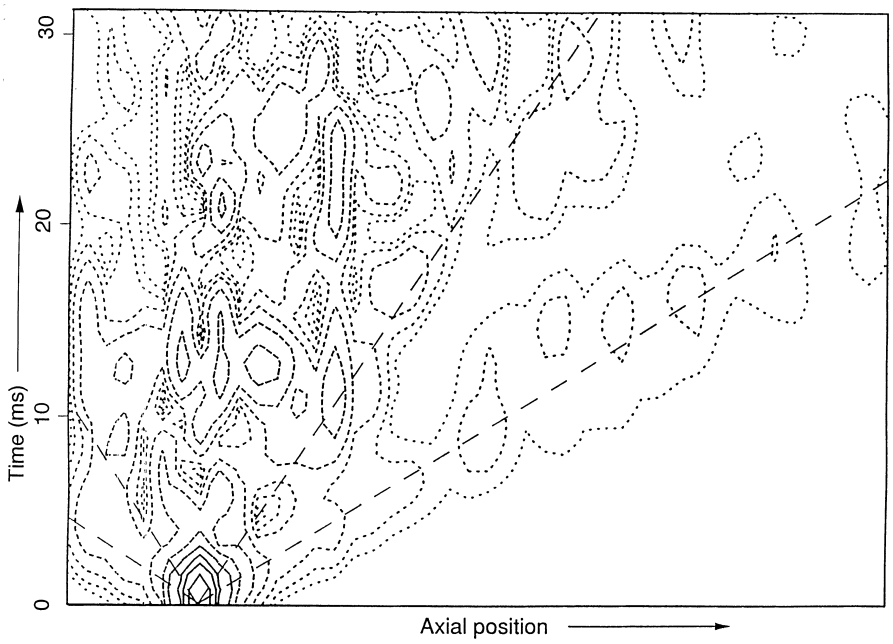

Fig. 10 Cross-section centred at 1562 Hz with bandwidth 156 Hz and 9 contours spaced at 3 dB intervals

remains the set of horizontal striations coming from band 1, as just explained, but instead of expanding in a wedge to fill the whole length of the cylinder, these lines are now confined to one end of the cylinder by an abrupt 'cliff' at bay 15. The reason for this is to be sought not in the theory of propagation of waves on an ideal, regular ribbed cylinder, but is a consequence of a fault in the construction of this particular structure. The plating of which the cylinder shell is made is welded in sections, and at bay 15 there is a significant misalignment of the plates through the welded joint. This misaligned joint acts as a strong reflector of waves at these higher frequencies, virtually confining all vibration to one end of the cylinder. This is an example of an important constructional feature whose consequences are made clear by the cross-section method, but which was unremarked previously.

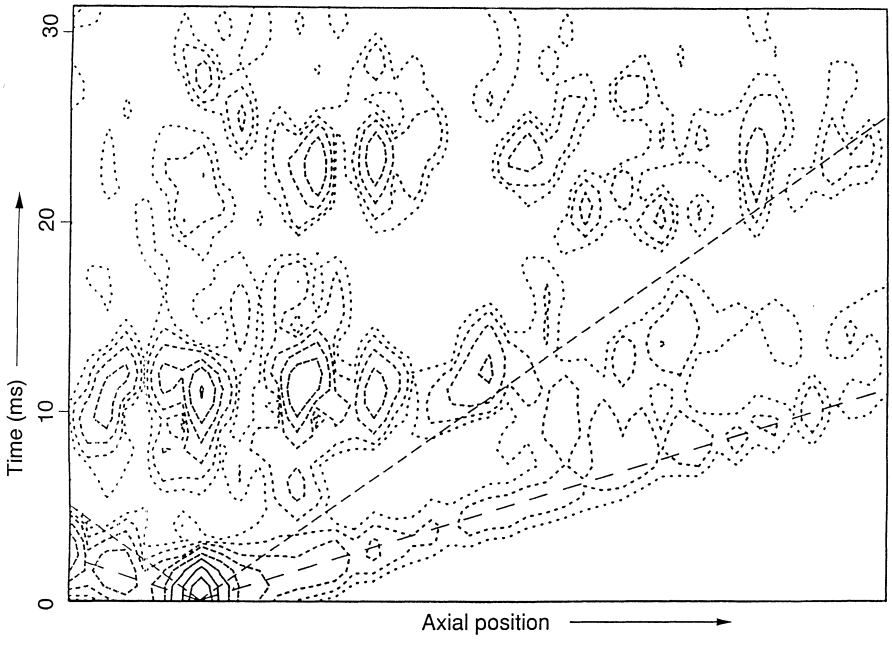

Fig. 11 Cross-section centred at 2031 Hz with bandwidth 156 Hz and 9 contours spaced at 3 dB intervals

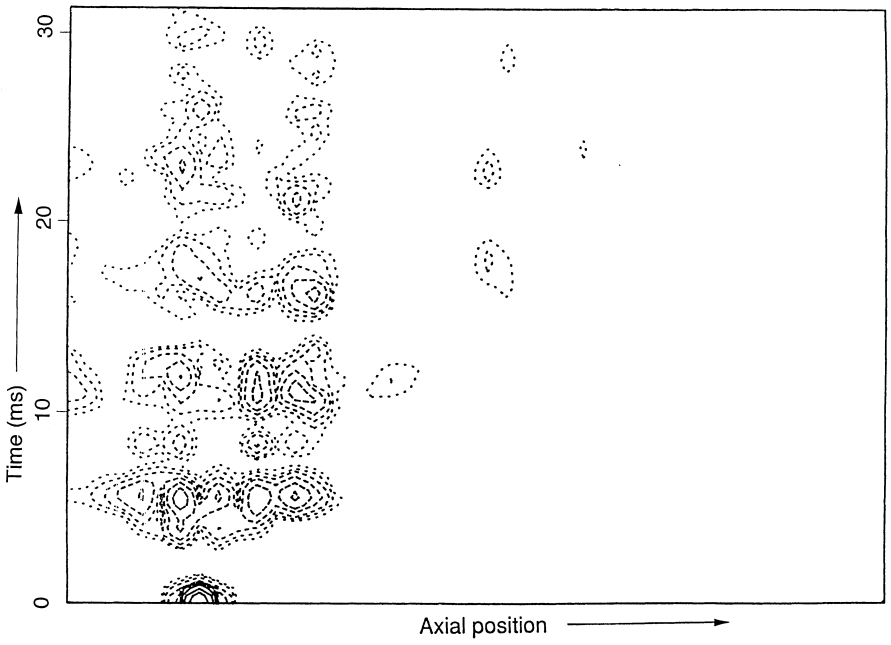

Fig. 12 Cross-section centred at 4062 Hz with bandwidth 312 Hz and 8 contours spaced at 3 dB intervals

5 END REFLECTIONS

Data presented previously [**3**] from an unribbed cylinder showed evidence of many reflections from the ends of the cylinder. However, such reflections are not clear for the ribbed cylinder, as the cross-sections from the previous section show. Only occasionally is it possible to identify a clear reflection, even from the end of the cylinder closest to the excitation, just 8 bays away from the excitation point. There are several possible reasons for this. It could be simply a result of the complexity of the problem, with the many different transmission mechanisms interfering with one another to obscure any simple patterns. Secondly, some of the dispersion curves change significantly on a frequency scale comparable with the frequency window width. This makes a simple wave-packet view inappropriate, since the details of the dispersion characteristic cannot be resolved sufficiently well. A third possibility concerns the dynamic behaviour of the partial-sphere end caps of the cylinder. These will have resonances of their own, and for frequencies close to these they will reflect incoming waves with a strongly frequency-dependent phase shift. This could disrupt wave-packets so that, after reflection, they no longer produced clear lines in the cross-section plot.

To focus on the second possibility above, consider the space–time response of a simple system with a pass-band structure. The simplest such model is a chain of identical oscillators, in which each is coupled in an identical way to its two neighbours [**4**]. First a chain of infinite length is considered and then one of finite length. In both cases the space–time impulse response function is calculated, with no frequency analysis. This will simulate the effect of a cross-section in which a single pass band lies entirely within the frequency window being used. Figure 13 shows the computed result for an infinite chain of coupled oscillators, plotted as a function of time and position in the same way as the experimental cross-sections. The structure of the disturbance that propagates from the impulse is clearly shown. After the initial wave-packet reaches a particular observing site, it is followed by a series of further arrivals of diminishing amplitude. This goes some way towards explaining why the pattern of Figs 11 and 12 fills the triangle between the first-arrival lines, since those figures apply to a frequency regime in which narrow bands are not resolved by the width of the frequency window in use.

There is a simple physical interpretation of the pattern shown in Fig. 13. After the first arrival, corresponding to the highest group velocity at the centre frequency of the pass band, slower components arrive from either side of the band centre. Because the group velocity pattern is symmetric about the band centre, any arrival time after the fastest arrival will be shared by waves at two different frequencies. An observer at a fixed point will thus receive two frequencies which move progressively apart from the band centre frequency towards the band edges. These frequencies will beat, and the beat frequency will tend towards the width of the pass band. Thus the observed motion is modulated at a frequency that tends to the pass band width, producing a series of wave-packets arriving in the wake of the first.

Figure 14 shows the result of a similar calculation for a finite chain of coupled oscillators. The model assumes 44 identical coupled oscillators driven initially at

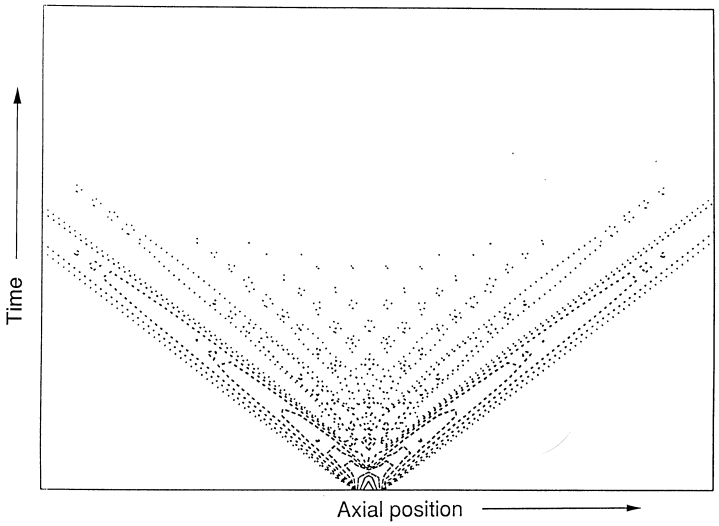

Fig. 13 Space–time plot of the impulse response of an infinite chain of identical coupled oscillators

number 8, so the contour plot is comparable in general terms with the cross-section pictures (although no attempt has been made to match any quantitative features of the ribbed cylinder by tuning model parameters). Fixed ends are assumed, so that the mode shapes along the chain are sinusoidal. This picture allows the boundary-reflection problem to be considered for a finite system with a pass band that is not resolved in frequency in a cross-section.

The early motion following the initial impulse is, of course, like that of Fig. 13 (but plotted on a different time-scale). Only when the first wavefront reaches one end of the system does the behaviour begin to differ from that of an infinite chain. Thereafter, energy begins to be reflected back, and this reflection gives rise to a complicated interference pattern, showing the slower components of the outgoing wave which have not yet reached the boundary. This goes some way towards explaining why coherent boundary reflections are not often seen in the cross-section pictures. In this case the reflected wave from the left-hand end of the chain can be seen fairly clearly, but it is accompanied by other lines radiating from the reflection point. The precise details of these lines are dependent on the assumed boundary conditions, but the existence of an interference pattern somewhat similar to this is inevitable when there is a spread of group velocities present. Once the waves reach the right-hand end of the chain and reflect again, the

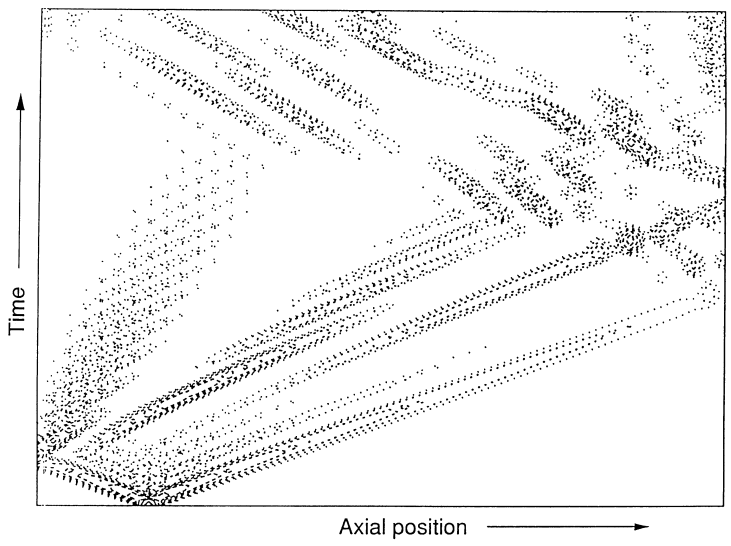

Fig. 14 Space–time plot of the impulse response of a chain of 44 coupled oscillators excited on oscillator 8. Fixed boundary conditions are assumed at both ends of the chain

multiple interference pattern is sufficiently complicated that only rather distant echoes of the simple pattern of Fig. 2a can be discerned.

6 CONCLUSIONS

Examination of space–time cross-section pictures obtained from a ribbed cylinder already studied in some detail [**1**, **2**] has increased understanding of the vibrational behaviour of that structure. The behaviour found did not contradict the earlier study, and in some ways confirms it rather convincingly. However, taking this different point of view has brought to light some new aspects of the behaviour. A constructional flaw of the cylinder, distortion in a welded joint, showed up with great clarity in the cross-sections at higher frequencies, the vibration being strongly reflected from this structural anomaly.

The underlying motive for studying cross-sections was to follow the progress of wave-packets in structures. This was successful to an extent, particularly for the fastest-propagating transmission mechanism in each frequency band. However, it has been demonstrated that interference between wave-packets can cause modulations in the sonograms obtained from individual points on the structure, and hence in the cross-sections calculated from them. The interference patterns can give interesting information in their own right, but they make the progress of wave-packets more difficult to trace in the cross-sections. Two major mechanisms of 'interference' were identified in this study:

1. When the analysis bandwidth encompasses a complete pass band, energy is not seen to propagate as a single, slowly dispersing wave-packet, but as a series of smaller wave-packets with slowly diminishing amplitude. This result was predicted by theoretical modelling and its effects were observed at higher frequencies. When this behaviour is combined with an end reflection, a complicated interference pattern results which can mask any clear lines of the reflecting initial wave-packet.
2. Closely spaced pass bands for adjacent values of angular order n produce a circumferential group velocity which is low enough to allow sonogram analysis to resolve each trip round the circumference by a wave-packet travelling on a helical path. This produced marked horizontal striations in the cross-sections at higher frequencies, since the measurements were made at a single line of sites along an axial line on the cylinder.

ACKNOWLEDGEMENTS

The authors thank many colleagues, especially Dr C. H. Hodges (now deceased), Dr I. Roebuck and Dr J. F. M. Scott, for invaluable discussions on this work. The work was carried out with the support of the Procurement Executive, Ministry of Defence.

REFERENCES

1 **Hodges, C. H.**, **Power, J.** and **Woodhouse, J.** The low frequency vibration of a ribbed cylinder. Part 1: theory. *J. Sound Vibr.*, 1985, **101**, 219–235.
2 **Hodges, C. H.**, **Power, J.** and **Woodhouse, J.** The low frequency vibration of a ribbed cylinder. Part 2: observations and interpretation. *J. Sound Vibr.*, 1985, **101**, 237–256.
3 **Hodges, C. H.**, **Power, J.** and **Woodhouse, J.** The use of the sonogram in structural acoustics and an application to the vibrations of cylindrical shells. *J. Sound Vibr.*, 1985, **101**, 203–218.
4 **Hodges, C. H.** and **Woodhouse, J.** Vibration isolation from irregularity in a nearly periodic structure: theory and measurements. *J. Acoust. Soc. Am.*, 1983, **74**, 894–905.

APPENDIX

To analyse the reactive enhancement at $t = 0$, first recall that the individual sonograms are obtained by windowing the velocity response time series and Fourier analysing the result. Since the window used is short compared with the damping time-scale, damping may be neglected here. In terms of normalized modes $\phi_k(x)$ with natural frequencies ω_k, the velocity response to an impulse applied at point y is

$$v(x, t) = \sum_k \phi_k(x)\phi_k(y)\ \cos(\omega_k t) \tag{1}$$

The sonogram signal is then given by

$$V(x, t, \omega) = \int_{-\tau}^{+\tau} v(x, t + t')f(t')\ \mathrm{e}^{\mathrm{i}\omega_k t'}\ \mathrm{d}t' \tag{2}$$

where $f(t)$ is the window function and τ is the half-width of the window. The Fourier transform of the function $f(t)$ in equation (2) defines a frequency filter, and only modes falling within its bandwidth contribute to the signal. In order to reduce the 'tails' of this filter a Hanning window has been chosen, $f(t) = 1 + \cos(\pi t/\tau)$. Because the signal is causal, the effective window is truncated at $t = 0$, and therefore the equivalent frequency filter is of a much wider bandwidth when $t < \tau$, allowing more modes to contribute and leading to an enhanced signal near the time origin.

If the signal were made non-causal by extrapolating it back to negative time, there would be no enhancement. The Fourier transform in equation (2) would then be entirely real, and its amplitude would be the same as the real part of the causal signal that actually needs to be dealt with (apart from a factor of 2). Thus the

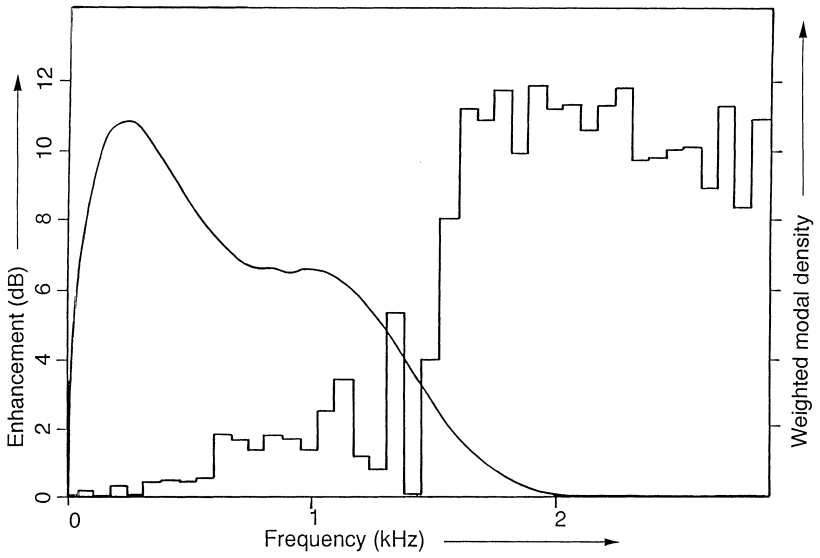

Fig. 15 The calculated signal enhancement due to reactive motion at the driving point. The modal density, weighted by the appropriate mode shape factors, is shown as a histogram

enhancement produced by the anomaly at $t = 0$ may conveniently be characterized by

$$\left|V(y, 0, \omega)/\mathrm{Re}[V(y, 0, \omega)]\right|^2 \tag{3}$$

However, from equations (1) and (2),

$$V(x, 0, \omega) = \tfrac{1}{2}\int \rho(\omega')[F(\omega + \omega') + F(\omega - \omega')]\, \mathrm{d}\omega' \tag{4}$$

where $F(\omega)$ is the Fourier transform of $f(t)$ and $\rho(\omega)$ is the modal density weighted by the appropriate squared mode shape factor. Using the known Fourier transform of the Hanning window function $f(t)$ together with a weighted modal density function computed using the theoretical model described in reference [**1**], the expected enhancement could thus be calculated. Results are shown in Fig. 15. The weighted modal density for the ribbed cylinder is plotted as a histogram, and the consequent enhancement at $t = 0$ appears as a smooth curve.